remote sensing

IMPACT FACTOR 4.2

CITESCORE 8.3

Article

Seasonal and Interannual Variations in Sea Ice Thickness in the Weddell Sea, Antarctica (2019–2022) Using ICESat-2

Mansi Joshi, Alberto M. Mestas-Nuñez, Stephen F. Ackley, Stefanie Arndt, Grant J. Macdonald and Christian Haas

Special Issue

Monitoring Sea Ice Loss with Remote Sensing Techniques

Edited by

Prof. Dr. Kohei Cho and Dr. Josefino Comiso

MDPI

https://doi.org/10.3390/rs16203909

remote sensing

MDPI

Article

Seasonal and Interannual Variations in Sea Ice Thickness in the Weddell Sea, Antarctica (2019–2022) Using ICESat-2

Mansi Joshi [1], Alberto M. Mestas-Nuñez [1,*], Stephen F. Ackley [1], Stefanie Arndt [2], Grant J. Macdonald [3] and Christian Haas [2,4]

[1] Department of Earth and Planetary Sciences, University of Texas at San Antonio, San Antonio, TX 78249, USA; mansi.joshi@my.utsa.edu (M.J.); stephen.ackley@utsa.edu (S.F.A.)
[2] Alfred-Wegener-Institut, Helmholtz-Zentrum für Polar- und Meeresforschung, 27570 Bremerhaven, Germany; stefanie.arndt@awi.de (S.A.); christian.haas@awi.de (C.H.)
[3] Department of Geography, Durham University, Durham DH1 3LE, UK; grantmac89@gmail.com
[4] Institute for Environmental Physics, University of Bremen, 28359 Bremen, Germany
* Correspondence: alberto.mestas@utsa.edu

Abstract: The sea ice extent in the Weddell Sea exhibited a positive trend from the start of satellite observations in 1978 until 2016 but has shown a decreasing trend since then. This study analyzes seasonal and interannual variations in sea ice thickness using ICESat-2 laser altimetry data over the Weddell Sea from 2019 to 2022. Sea ice thickness was calculated from ICESat-2's ATL10 freeboard product using the Improved Buoyancy Equation. Seasonal variability in ice thickness, characterized by an increase from February to September, is more pronounced in the eastern Weddell sector, while interannual variability is more evident in the western Weddell sector. The results were compared with field data obtained between 2019 and 2022, showing a general agreement in ice thickness distributions around predominantly level ice. A decreasing trend in sea ice thickness was observed when compared to measurements from 2003 to 2017. Notably, the spring of 2021 and summer of 2022 saw significant decreases in Sea Ice Extent (SIE). Although the overall mean sea ice thickness remained unchanged, the northwestern Weddell region experienced a noticeable decrease in ice thickness.

Keywords: ICESat-2; sea ice thickness; Weddell Sea

Citation: Joshi, M.; Mestas-Nuñez, A.M.; Ackley, S.F.; Arndt, S.; Macdonald, G.J.; Haas, C. Seasonal and Interannual Variations in Sea Ice Thickness in the Weddell Sea, Antarctica (2019–2022) Using ICESat-2. *Remote Sens.* **2024**, *16*, 3909. https://doi.org/10.3390/rs16203909

Academic Editor: Yi Luo

Received: 11 September 2024
Revised: 14 October 2024
Accepted: 18 October 2024
Published: 21 October 2024

1. Introduction

Sea ice thickness measurements are important for evaluating heat and salt budgets and improving sea ice projections in coupled climate models [1,2]. Information on sea ice thickness combined with sea ice extent also enables estimates of total ice volume, which is an important indicator of climate change [3,4]. Due to the linkages between sea ice variability and climate, understanding sea ice formation and growth, and therefore variations in sea ice thickness, are of key importance [5]. Antarctic sea ice extent had exhibited an increasing trend since satellite observations became available in 1978 but started to decline sharply around 2014 [6,7]. The areal loss of Antarctic sea ice extent in four years (2014–2017) exceeds the total loss by Arctic sea ice cover in 40 years. Antarctic sea ice reached its lowest maximum annual extent in the 45-year satellite record in September 2023 [8] (https://nsidc.org/news-analyses/news-stories/antarctic-sea-ice-hits-record-low-maximum-extent-2023); URL accessed 14 March 2024.

A similar analysis of annual sea ice extent over the last 40 years for the Weddell Sea shows consistency with the overall Antarctic trends, with the annual sea ice extent increasing until 2016 and then decreasing. Seasonally, the minimum monthly ice extent occurs in February, while the maximum monthly ice extent varies from August to October [6]. While there was a positive trend in extent in the Austral summer and fall before 2014, there was a negative trend in extent in the Austral winter and spring. Because annual sea ice formation in the Weddell Sea accounts for 5–10% of total Antarctic sea ice production, the

region is a significant source of Antarctic Bottom Water (AABW) [9]. The western Weddell has ice year-round, whereas the eastern Weddell shows the characteristics of seasonal sea ice. Thus, it is important to measure seasonal and interannual sea ice variability in the Weddell Sea to better quantify and understand its role in the global climate [10].

Numerous past studies have estimated in Arctic sea ice thickness from radar or laser altimetry, but there are fewer studies of this kind in Antarctica. There are two main reasons for the uncertainty in estimating Antarctic sea ice thickness from altimetry. First, freeboard estimates of Antarctic sea ice are difficult because the thicker Antarctic snow layer can depress the ice and cause flooding, complicating the conversion of ice elevation into freeboard [11–14]. Second, snow depth distribution over Antarctic sea ice is not as widely known as for Arctic sea ice [13,15]. In the Arctic, there are also more extensive measurements of sea ice thickness from a series of in situ transects by nuclear submarines with mounted upward-looking sonars, from drifting buoys, and from moorings of upward-looking sonars [16–18]. In Antarctica, however, direct sea ice thickness measurements are limited due to the lack of nuclear submarine transects and the relative lack of field and aerial campaigns compared to the Arctic.

Measurements of sea ice thickness may alternatively involve active and passive microwave satellite data. Passive microwave sensors measure the brightness temperature, which has been used to derive the thickness of thin ice, thinner than ~0.2 m. An example of a passive microwave sensor is the Soil Moisture and Ocean Salinity (SMOS) satellite, which operates at the L-band and is also used to obtain Antarctic Sea ice thickness up to 1 m [19–22]. Active sensors include Envisat, which is equipped with a Ku-band radar altimeter and uses the backscatter signal returned from the snow–ice interface. There are significant errors in retrieval from Envisat when snow is wet and not cold, and in addition, the radar altimeter has a large footprint size of around 2–10 km. These shortcomings in radar freeboards affect the ability to resolve local sea surface height during the freeboard retrieval [23].

Laser altimetry retrieves the elevation above sea level of the top surface of the snow on sea ice, termed 'total freeboard', in contrast with radar altimetry (e.g., CryoSat-2), which reflects from the top ice surface, thus measuring 'ice freeboard'. Ice thickness can be calculated from freeboard by considering isostatic balance. The Ice, Cloud, and land Elevation Satellite (ICESat), which operated from 2003 to 2009, was the first satellite-based laser altimeter to measure sea ice total freeboard (~70 m footprint diameter) and many studies have converted these estimates into thickness [5,7,17,19,24–26]. The ICESat mission ended in fall of 2009 and was followed by ICESat-2, which was launched in 2018, leaving a gap between the two missions. This gap was partially filled by the NASA Operation IceBridge (OIB) airborne campaigns, which studied parts of the west Antarctic region annually during Oct-Nov from 2009 to 2017. A previous study [7] combined these observations from ICESat and OIB and produced a long-term record of total freeboard and ice thickness from 2003 to 2017 in the Weddell Sea. In these observations, sea ice thickness did not show any statistically significant trend; however, they observed a decreasing trend for ice extent from 2014 to 2016.

Photon-level point cloud data from NASA's ICESat-2 provides us with unique capabilities to analyze changes in ice thickness at fine spatial (20 m) and temporal (weeks to months) scales. In this paper, we estimate sea ice thickness from ICESat-2 using an empirical approach. These results are then compared with ground-based measurements to better understand the role of snow depth in empirical equations for ice thickness estimations and the comparison with coincident ship-based and ground-based electromagnetic (EM) thickness measurements in the Weddell Sea. We analyze the ICESat-2 data over the Weddell Sea to understand the changes in sea ice thickness in recent years compared to the previous analyses in the context of recent changes in sea ice extent. The Weddell Sea region that will be studied is presented in Figure 1a superimposed on a color contour map of sea ice concentration for January 2022 from the National Snow and Ice Data Center (NSIDC, https://masie_web.apps.nsidc.org/pub/DATASETS/NOAA/G02135/south/

monthly/geotiff/01_Jan/); URL accessed 7 October 2024. In Figure 1b, the study area is expanded to illustrate the ICESat-2 observational coverage and to present the locations of the ground-based observations that will be used for comparison.

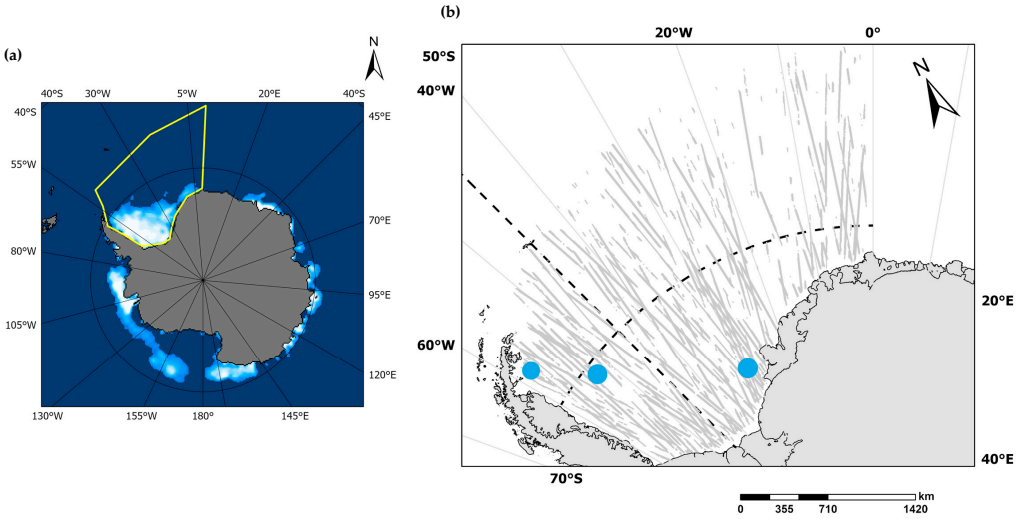

Figure 1. (**a**) Sea ice concentration from NSIDC for Antarctica in January 2022 with solid dark blue depicting ice concentrations smaller than 15% and white indicating 100% ice. The study area in the Weddell Sea is indicated by the yellow polygon. (**b**) Expanded study area map showing the location of ICESat-2 tracks for September 2022. Also shown are the 45°W meridian, which divides the study area into eastern and western sectors, and the 68°S parallel, which further divides the western sector into northwestern and southwestern regions, for the purpose of this study. The solid blue dots indicate the approximate locations of the field observations used in this study, which were obtained from 2019 to 2022.

2. Data and Methods

2.1. Sea Ice Freeboard Observations from ICESat-2, Temperature Data and Study Area

The Advanced Topographic Laser Altimeter System (ATLAS) on board ICESat-2 uses three beam pairs to profile the earth's surface, each separated by a ~3.3 km distance cross track. Each pair consists of a strong and a weak beam spaced 90 m apart. The pulse energies of the strong beams are four times that of the weak. The pulse repetition rate of each beam profile is 10 kHz, and the footprints are 17 m in diameter [27,28]. The along-track freeboard data used here are from the ICESat-2 ATL10 product (Release 005) from the National Snow and Ice Data Center [29]. The ATL10 product provides estimates of sea ice freeboard with a variable along-track resolution of 20–200 m, with each segment consisting of 150 returned signal photons [30,31]. Sea ice and sea surface elevations from the ATL07 product are used to derive the freeboard estimates of the ATL10 product. Freeboards in ATL10 are calculated only where the ice concentration is greater than 50% and where the height samples are at least 25 km away from the coast to avoid uncertainties in coastal tide corrections [28].

The study area considered for this analysis is the Weddell Sea region from 0° to 55°W (Figure 1), and the region is divided into western (45°W–55°W) and eastern segments (0°W–45°W) [5]. Only the strong beam tracks are considered for the study.

2.2. Sea Ice Thickness Estimates from ICESat-2 Freeboard Observation

Sea ice thickness is calculated using the buoyancy principle by assuming that water, ice, and snow are in isostatic equilibrium [5,7].

In this study, we will estimate the sea ice thickness using the Improved Buoyancy Equation as follows (BOC) [4,7].

$$I = \frac{\rho_w F - (\rho_w - \rho_s)S}{\rho_w - \rho_i} \quad (1)$$

where I is the sea ice thickness, ρ_w, ρ_i and ρ_s are densities of water, ice, and snow respectively, F is total freeboard height from the ICESat-2 ATL10 product, and S is the snow depth derived from the empirical parameters c and d using Equation (2).

$$S = c + d \times F \quad (2)$$

These empirical parameters that relate snow depth to total freeboard (Table 1) are based on 174 profile mean values from 15 ship cruises from 1986 to 2007 in the Antarctic Sea ice zone [4,7,32]. Freeboards greater than two meters are not considered for analysis to avoid the possible effects of icebergs and to remove any outliers. The densities used in this study are 1023.9, 915.1, and 300 kg m^{-3} for water, ice, and snow, respectively [5,17,19,26].

Table 1. The empirical parameters from Equation (2) [4].

Sea Sector	c (cm)	d
Western Weddell	0.9	0.88
Eastern Weddell	−1.0	0.87

For statistical analysis, the variable height segment is considered, by weighting the data based on the segment length, and the mean thickness ($\bar{h}$) within a given area is estimated using Equation (3), where h^i is the thickness of a given segment, L^i is the segment length, and N is the number of segments in a given area/bin/grid cell [2,33].

$$\bar{h} = \frac{\sum_N h^i L^i}{\sum_N L^i} \quad (3)$$

2.3. Sea Ice Thickness Estimates from Field Observations

The field measurements used in this study (Figure 1b) were carried out by the German Research ice breaker RV *Polarstern* in 2019 and 2021 from January to March. The northwestern Weddell pack ice was sampled in 2019, and the southeastern part of the Weddell pack ice was sampled in 2021. A GPS-equipped Magna Probe system (Snow-Hydro, Fairbanks, Alaska, USA) was used, which consists of a ski pole-like rod that contains a magnetostrictive device. Attached to this rod is a basket and magnet assembly slide. The basket floats on the snow, and the rod is inserted into the snow's base. When a button is pushed, it measures the distance between the rod tip and basket along with the position [34]. A GPS-equipped Magna Probe with a horizontal resolution of 1–2 m was used to measure snow depth. The total sea ice thickness was measured using ground-based multi-frequency electromagnetic induction measurements.

As a part of the Endurance 22 expedition of the Alfred Wegner Institute (AWI), which aimed at measuring Antarctic sea ice properties, the thickness of the ice was measured from 15 February to 8 March 2022 from the *S.A. Agulhas II* icebreaker vessel using an electromagnetic induction instrument (EM) suspended above the ice surface during the ship's travel through the ice. This method typically uses an airborne device, which uses electromagnetic induction sounding with laser altimetry and relies on the difference in the electrical conductivity between sea ice and water [35–38]. For the icebreaker measurements, a Geonics EM-31 instrument (Geonics Limited, Toronto, Canada) with two antenna coils spaced 3.66 m apart operating at a frequency of 9.8 kHz was used to measure the electrical conductivity. The difference between the ice–water interface and the snow or ice interface is used to calculate the total ice thickness (sum of snow and ice thickness) (https://endurance22.org/uploads/2022/06/Science_Report_Endurance22_final_version.pdf); URL accessed 21 October 2023.

2.4. Temperature Data and Data from Previous Litretaure

ERA5, which has replaced ERA-Interim, is the fifth-generation European Centre for Medium-Range Weather Forecasts (ECMWF) reanalysis of the global climate and weather

for the past 8 decades. ERA5′s monthly averaged 2 m air temperature data with a resolution of 0.25° were collected over the Weddell region from 2019 to 2022. The sea ice thickness from present data are also compared with previous literature to better understand the changes with respect to previous' years data [5,7,9,23,26,28,39,40]. In this paper, we examined the primary factors that are associated with ice variability. A more in-depth analysis of the drivers behind ice changes is beyond the scope of this study and will be addressed in a future publication.

3. Results and Discussion

3.1. Freeboard Comparison of Western and Eastern Weddell Sea Sectors (2019–2022)

Maps of ICESat-2 total freeboard and their modal distributions in the Weddell Sea for different seasons are shown in Figure 2. The seasons are classified as January to March (summer), April to June (autumn), July to September (winter), and October to December (spring) [9,41]. Figure 2a–p shows that the eastern Weddell Sea exhibits seasonal growth in summer to maximum total freeboard extent and values in late winter. In contrast, the western Weddell Sea maintains similar freeboard extent and values throughout the year and represents one of the largest regions of Antarctic Sea ice during the summer, containing multiyear ice. The observed distribution is thus consistent with sea ice that is formed in the eastern sector being advected clockwise around the southern Weddell Sea (cyclonic gyre) and subsequently exported through the northwestern boundary after its transit [28]. The modal values in freeboard in the eastern region (Figure 2r) shift from 0 to 0.1 m in summer towards a higher value of 0.15 to 0.2 m in winter and spring. This behavior suggests that sea ice grows from July to December, and then it is transported to the western Weddell region. In the western Weddell (Figure 2q), two modal values are observed during the summer and spring seasons. The first modal value at about 0 m indicates the formation of new sea ice, while the second modal value at 0.2–0.43 m represents multiyear sea ice, indicative of thicker ice. The mean freeboard in the western Weddell ranges from 0.3 m to 0.5 m, indicating a higher freeboard compared to the eastern Weddell. Figure 2a–p also shows that the northwestern Weddell has higher freeboard values throughout the year.

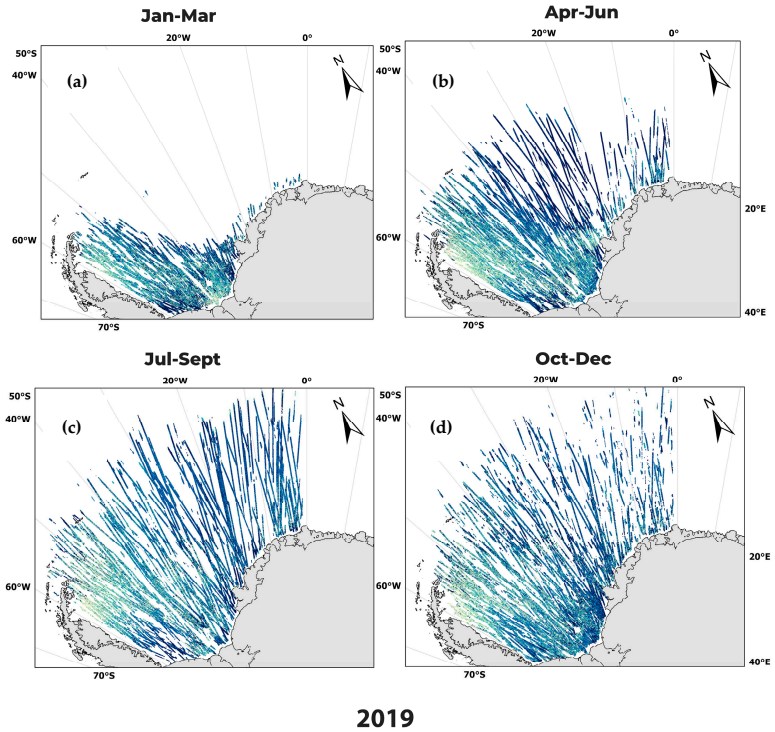

Figure 2. *Cont.*

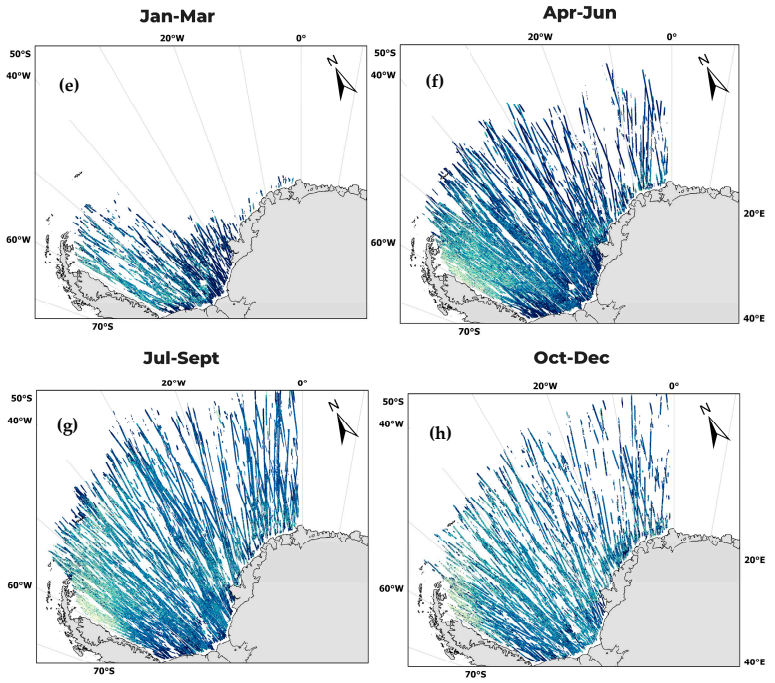

Figure 2. *Cont.*

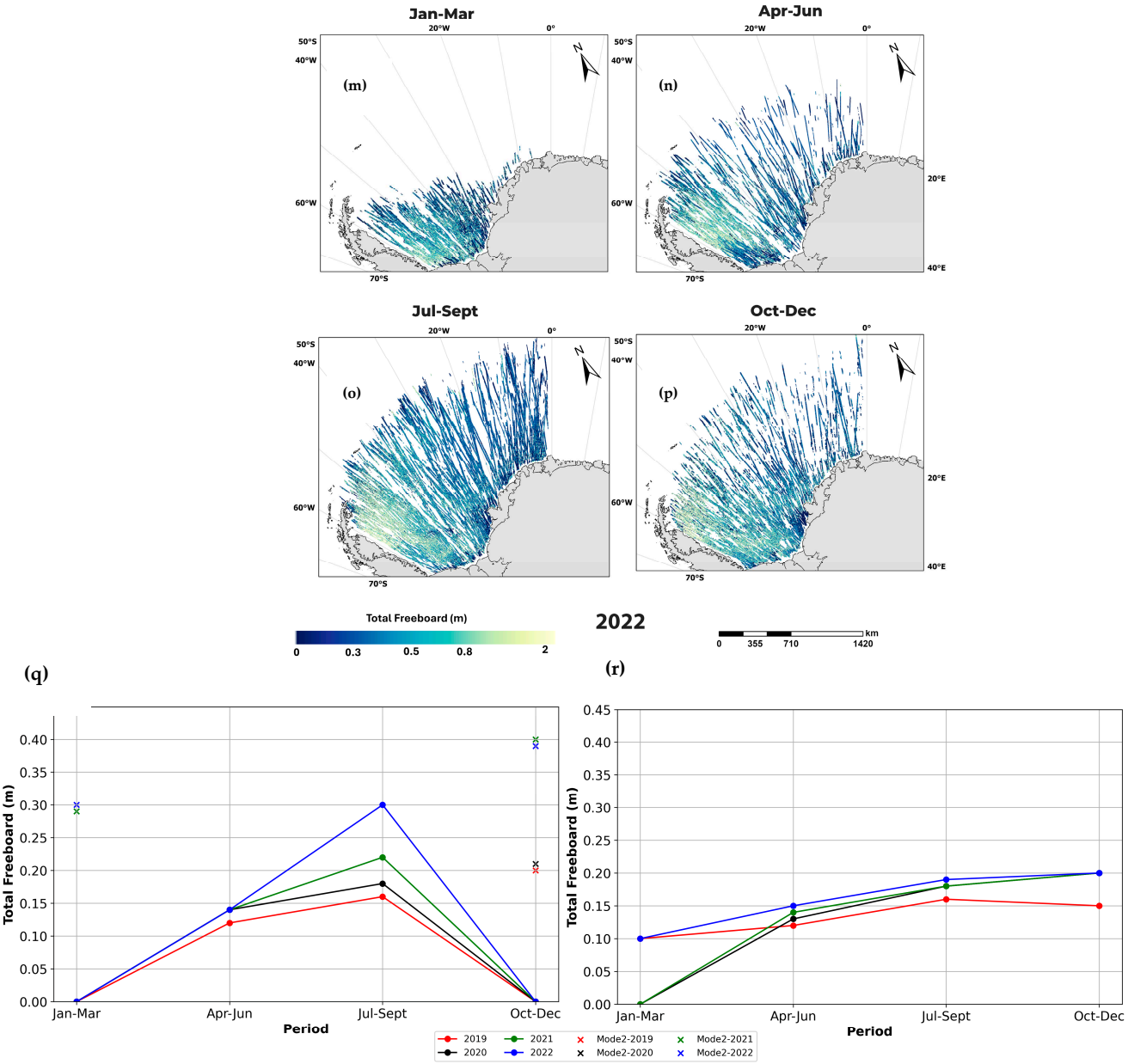

Figure 2. (**a**–**p**) Multi-panel maps of the study area showing ICESat-2 total freeboard tracks from 2019 to 2022 for different seasons. The bottom two panels show: (**q**) the modal values of freeboard in meters for the western Weddell (solid color circles) with second modal values shown by the color crosses, 2019 (red), 2020 (black), 2021 (green), and 2022 (blue); and (**r**) the same as (**q**) but for the eastern Weddell.

The uncertainty in the ICESat-2 total freeboard retrievals was about 0.02–0.04 m [2]. During the Operation IceBridge Arctic deployment in 2019, surface height and total freeboard products of ICESat-2 (ATL07 and ATL10) were assessed with near coincident retrievals from Airborne Topographic Mapper (ATM) lidar. In Antarctica, similar analyses were carried out for ATM data [7]. The footprint size of ATM altimetry data is about 1 m, which is close to the footprint size of ICESat-2, i.e., 17 m. The study observed an accuracy of about 0.05 m in sea surface height and total freeboard [7]. Thus, from the above uncertainty analysis [7] from Antarctica, the freeboard uncertainty can range from 0.02 to 0.05 m.

Thick snow in the Antarctic region can weigh down and immerse sea ice in seawater, forming a flooded snow layer. As ICESat-2 measures the snow and ice height above the sea surface, the flooded snow can be a reason for uncertainty in the ice thickness estimations

using the empirical approach. The explanation provided in [7] highlights how the flooded snow acts like ice in density and thus makes the present method of estimating sea ice thickness robust in dry snow layer depth and ice thickness. To understand more, the snow depth data from a previous study were analyzed. The study in [28] uses differences in freeboard data from ICESat-2 and CryoSat-2 collected between April and November 2019 to estimate snow depth, based on the assumption of zero freeboard. The snow depth estimates from this study in the western Weddell are compared as they are spatially similar to the findings in their analysis. The study in [28] uses ICESat-2 data at a lower resolution, which limits the direct validation of their data. A spatial comparison of the snow depth from different methods is made to understand its role in thickness estimations (Table 2). The snow depth from the ICESat-2 and CryoSat-2 differences are lower than the empirical method, and thus, the ice thickness estimates are higher. The snow depth from the empirical approach is closer to the total freeboard, and we hypothesize, therefore, that the empirical method provides a better estimate of sea ice thickness.

Table 2. Freeboard and snow depth estimates from April to November 2019.

ICESat-2, CryoSat-2 Difference [28]		**April**	**May**	**June**	**July**	**August**	**September**	**October**	**November**
W-Wedd	Freeboard (m)	0.365 ± 0.2	0.411 ± 0.19	0.362 ± 0.17	-	0.387 ± 0.197	0.38 ± 0.192	0.382 ± 0.2	0.395 ± 0.18
	Snow depth (m)	0.2 ± 0.138	0.22 ± 0.12	0.20 ± 0.12	-	0.225 ± 0.14	0.225 ± 0.14	0.227 ± 0.16	0.22 ± 0.13
ICESat-2 (empirical equation)									
W-Wedd	Freeboard (m)	0.35 ± 0.24	0.40 ± 0.25	0.35 ± 0.25	-	0.39 ± 0.25	0.37 ± 0.25	0.38 ± 0.25	0.38 ± 0.24
	Snow depth (m)	0.32 ± 0.21	0.36 ± 0.22	0.32 ± 0.22	-	0.35 ± 0.22	0.33 ± 0.22	0.34 ± 0.22	0.34 ± 0.21

3.2. Estimating Sea Ice Thickness from ICESat-2 Using the Empirical Formula

Figure 3 shows sea ice thickness distributions from 2019 to 2022. The left and right panels represent the western and eastern Weddell sectors, respectively. In the western Weddell, sea ice thickness ranges up to 7 m during the peak sea ice formation times of the year, i.e., from July to December. In the eastern Weddell, during the same period, thicknesses range up to 5 m.

The interannual variation of sea ice thickness in the eastern Weddell is small over the time period of 2019–2022, showing no clear trend. Similar results were reported by [7] in a long-term record from 2003 to 2017. The western Weddell generally exhibits a bimodal distribution during the summer and spring seasons, as detailed in the freeboard section. The highest modal and mean values, 1 m and 1.84 m, respectively, were observed in 2022 for the western Weddell region. The longer tail of the distribution, along with the bimodal values, indicates more deformed ice in the western Weddell compared to the eastern region. In 2020, the mean sea ice thickness decreased from the previous year, 2019, during summer, autumn and winter (January to September) in both the western and eastern Weddell regions. In 2019, the mean thickness in the western Weddell ranged from 1.21 m to 1.61 m, but it decreased in 2020, with the range narrowing to 1 m to 1.24 m. Similarly, in the eastern Weddell, the mean thickness observed in 2019 ranged from 1.18 m to 0.92 m, further declining in 2020 to a range of 0.66 m to 0.99 m. In the western Weddell, this decrease in mean sea ice thickness was also observed during spring 2020 (October to December). During summer, from 2019 to 2022, both regions consistently showed lower mean sea ice thickness compared to other months, indicating thinner ice during the summer. The seasonal variation in the eastern Weddell region remained similar across all four years. Sea ice is at its minimum in summer, begins to grow towards autumn and winter, and remains at its maximum until spring. The eastern Weddell shows to exhibit higher mean sea ice thickness in October with values ranging from 1 ± 0.78 m to 1.25 ± 0.89 m, while the western Weddell has higher thickness values from July to December (Figure 3, left). The sea ice thickness in the eastern region increased, and the western part of the Weddell subsequently became thicker after 2020. This pattern is consistent and can be seen across

all years from 2019 to 2022. The seasonal variation in the eastern Weddell region does not show any significant pattern from 2019 to 2022.

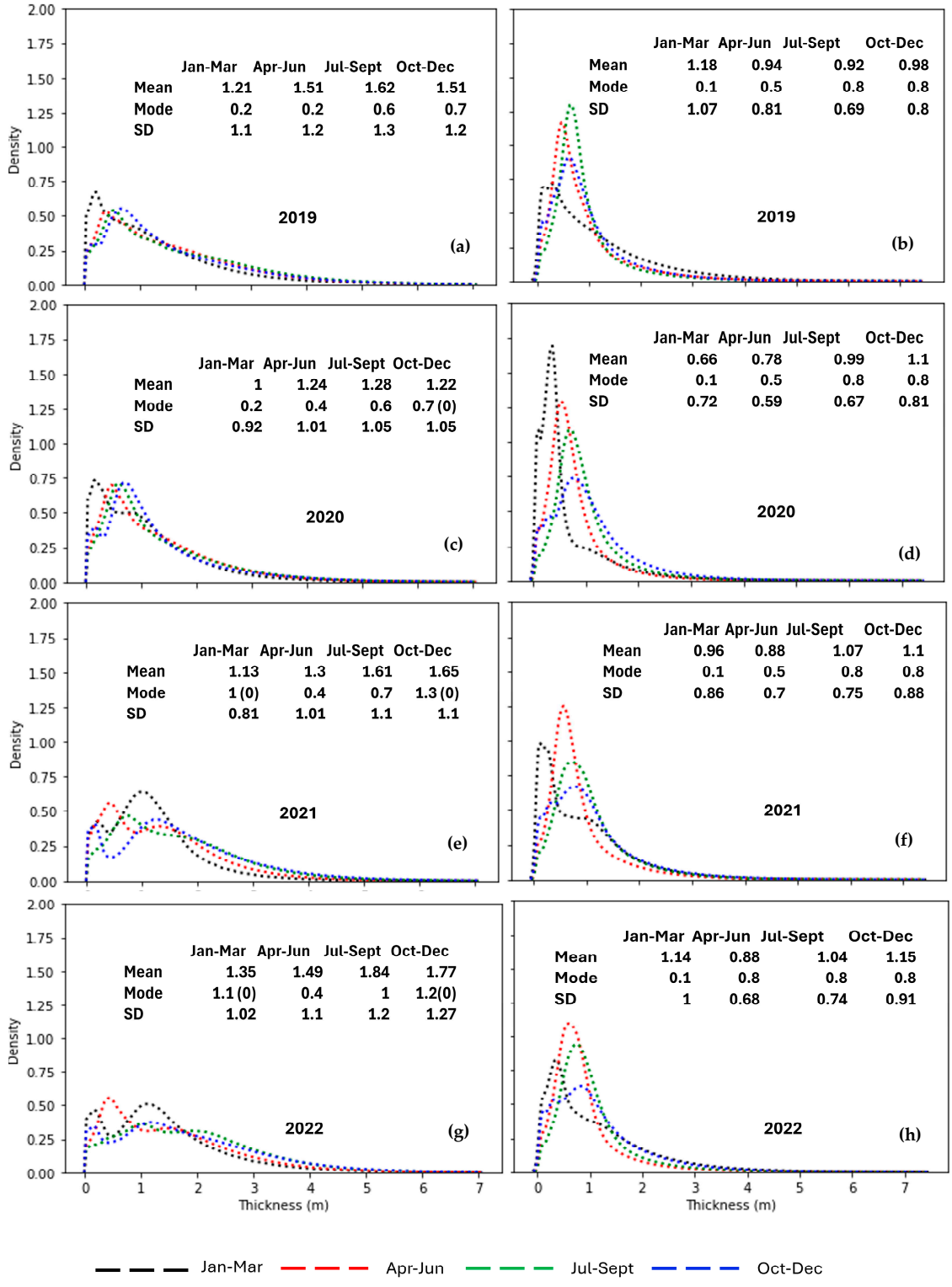

Figure 3. Thickness estimates of the western Weddell (**left**—**a**,**c**,**e**,**g**) and eastern Weddell (**right**—**b**,**d**,**f**,**h**) regions from 2019 to 2022. Mean, mode, and Standard Deviation (SD) in meters. Bimodal mode values in the western Weddell are depicted in parenthesis.

The ICESat-2 results from the present study are compared with previous literature [39]. These results are used to compare the thickness estimates with the same satellite data i.e., ICESat-2 in the same area in Weddell, but with two different algorithms for converting total freeboard to thickness. The comparable thickness from ICESat-2 with previous literature helps in validating and thus, explaining the changes in sea ice thickness since 2019. The improved One Layer Method (OLMi) was applied to estimate sea ice thickness using ICESat-2 data from [39]. In Table 3, the mean thickness shows a difference of 0.2–0.3 m in the months of Jan-Mar in the eastern Weddell, whereas the western Weddell shows a difference of 0.1–0.4 m (Table 3) when compared to the Improved BOC method used here.

Table 3. Comparison of mean thickness estimates and Standard Deviation (SD) in meters with [39] from January 2019 to July 2020. Icesat-2 as IS2 and eastern Weddell and western Weddell as EW and WW. Xu 21 study from [39].

Mean ± SD (EW)	Jannuary	February	March	April	May	June	July	August	September	October
IS2	0.8 ± 0.88	1.01 ± 0.97	0.89 ± 0.8	0.86 ± 0.71	0.88 ± 0.7	0.84 ± 0.66	0.89 ± 0.64	1.01 ± 0.64	1.04 ± 0.69	1.14 ± 0.77
Xu 21	1.03 ± 0.82	1.11 ± 0.9	0.86 ± 0.8	0.83 ± 0.68	0.81 ± 0.58	0.78 ± 0.55	0.83 ± 0.51	0.83 ± 0.51	0.94 ± 0.6	0.95 ± 0.7
Mean ± SD (WW)										
IS2	1.13 ± 1.02	1.06 ± 1.0	1.12 ± 0.9	1.31 ± 1.05	1.43 ± 1.1	1.35 ± 1.1	1.54 ± 1.1	1.64 ± 1.1	1.54 ± 1.1	1.28 ± 1.2
Xu 21	1.19 ± 0.88	1.05 ± 0.85	1.08 ± 0.8	1.24 ± 0.88	1.25 ± 0.87	1.24 ± 0.84	1.45 ± 0.97	1.48 ± 1.02	1.39 ± 1	1.5 ± 1.04

3.3. Comparing ICESat-2 Estimates of Sea Ice Properties with Field Data

The ICESat-2 thickness, snow depth, and freeboard values are compared to the corresponding *Polarstern*'s measurements from the field campaigns of 2019, in the northwestern Weddell, and snow depth values of 2021 from the southeastern Weddell. In addition, the ICESat-2 sea ice thickness is compared to the corresponding *S.A. Agulhas II* icebreaker observations of 2022 in the western Weddell region. Figure 4 shows the locations of the field measurements (blue dots) and of the ICESat-2 satellite observations (red dots) taken around the same time and using the minimum distance varying between 10 and 100 km to the field data.

In the 2019 comparison, the data in the northwestern Weddell is divided into northwestern1 (NW1) and northwestern2 (NW2), referred to as southwestern and northwestern in [42]. The field measurements are from airborne and ground observations. The mean thicknesses observed in NW1 and NW2 from airborne measurements are 4.12 ± 1.87 m and 1.62 ± 1.05 m, with a modal thickness of 3.9 m and 0.9 m, respectively. Ground measurements using GEM showed a similar tendency, with mean thickness decreasing from 4.08 ± 2.03 m in NW1 to 1.5 ± 0.48 m in NW2. The ICESat-2 data observed a consistent latitudinal gradient, with mean thickness of 1.58 ± 0.81 m in NW1 and 1.16 ± 0.79 m in NW2. The snow depth values in NW1 and NW2 from the Magna Probe were 0.46 ± 0.29 m and 0.05 ± 0.06 m, while those from ICESat-2 using an empirical equation were 0.41 ± 0.2 m and 0.31 ± 0.19 m. Notably, mean snow depth values compare better in the NW1 location where values are higher, while in the NW2 location, the snow depth is overestimated by the empirical equation. This discrepancy could be attributed to the superimposed ice not being considered in the empirical equation. The total freeboard values, however, compare reasonably well at the two locations. In NW1, the freeboard from ice core measurements is 0.5 ± 0.4 m and from ICESat-2 is 0.46 ± 0.22 m. In NW2, the freeboard from ice core measurements is 0.43 ± 0.18 m and from ICESat-2 is 0.34 ± 0.22 m. There were two dates when the ICESat-2 tracks and the field measurements were taken around the same time and area: 1 March 2019 and 16 March 2019. The freeboard and thickness values from 1 March 2019 are close to field measurements showing 0.5 ± 0.4 m and 1.86 ± 0.95 m, and ICESat-2 showing 0.46 ± 0.22 m and 1.58 ± 0.81 m, respectively. However, there is no consistent pattern in field and ICESat-2 data showing similar values around lower or higher snow depth areas.

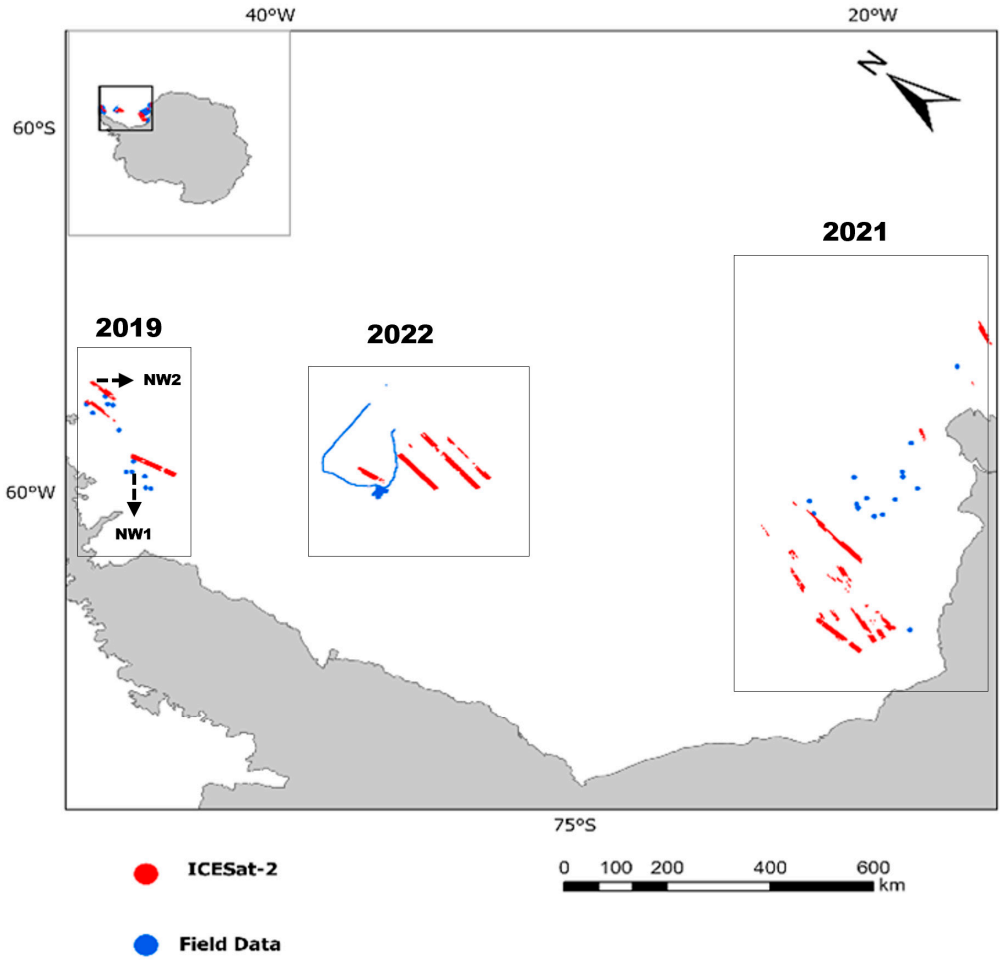

Figure 4. Location of ICESat-2 tracks in red with field data in blue. Field data from 2019 and 2021 are point measurements. The data from 2022 are thickness measurements on board Endurance 22 ship EM data.

In the 2021 comparison, the snow depth values from the field were 0.35 ± 0.22 m, whereas ICESat-2derived values were 0.17 ± 0.19 m. The differences could be due to the uncertainties introduced by the sampled areas not being the same. The sampling bias and time of day around which ICESat-2 and field values are considered can add to the differences in the measurements.

In the 2022 comparison, the sea ice thickness modal values are similar: 0.54 m for field and 0.6 m for ICESat-2 data. The mode of sea ice thickness depicts the growth of level ice. The agreement indicates that the field measurements of sea ice thickness from the EM provide some validation of the empirical approach used to estimate sea ice thickness from ICESat-2 freeboard. ICESat-2 does show a similar ice type, as described in the field data. To better understand the discrepancies in the dataset, it is essential to have field measurements taken at the same time as ICESat-2 data. This approach, as seen from the comparison on 1 March 2019, would help us use satellite data and modeling to better understand sea ice conditions on a larger scale.

3.4. Analysis of the Estimated Variability from 2019 to 2022

The extent of the ICESat-2 tracks decreases towards the spring of 2021 and the summer of 2022 because of the low sea ice extent (SIE) that occurred then. In [43], they discussed the low SIE observed in 2022 in the Southern Ocean. According to [43], the SIE has been decreasing since October 2021. The minimum extent in the Weddell Sea in 2022 was 1.09×10^6 km^2, which was the 12th lowest SIE, with the lowest being 0.78×10^6 km^2 on

20 February 1999 [43]. This can also be observed in Figure 2, where the extent of ICESat-2 tracks during Oct-Dec is less in 2021 (Figure 2l) and 2022 (Figure 2p) as compared to 2020 (Figure 2h). However, there were not any significant changes in the mean freeboard and thickness values during the same periods. Long term data are needed to establish the relationship between lower SIE and thickness values. Southwestern Weddell exhibits higher freeboard values, indicating the transport of sea ice from the southeastern Weddell towards the southwestern Weddell. Despite the decrease in SIE in 2022, [43] discusses the thinning of sea ice in the northwestern Weddell due to strong warm air over the Antarctic Peninsula. However, the mean thickness may not be affected due to the presence of multiyear sea ice in the western Weddell Sea.

For a more detailed understanding of the region, we divided western Weddell at 68°S into northwestern and southwestern Weddell. The western Weddell is the region with older ice, and thus, only the western Weddell is further divided into the northern and southern regions. Figure 5 shows the thickness difference between the northwestern and southwestern Weddell. Both regions show a decrease in thickness in 2020. In the summer of 2022 in northwestern Weddell, the mean thickness values are significantly lower (0.75 m) than in the previous year's summer thickness of 2021 (1.04 m) in that region. This indicates that, although the overall mean might not be affected because of the multiyear sea ice, parts of the region are experiencing low thickness values along with a decrease in SIE.

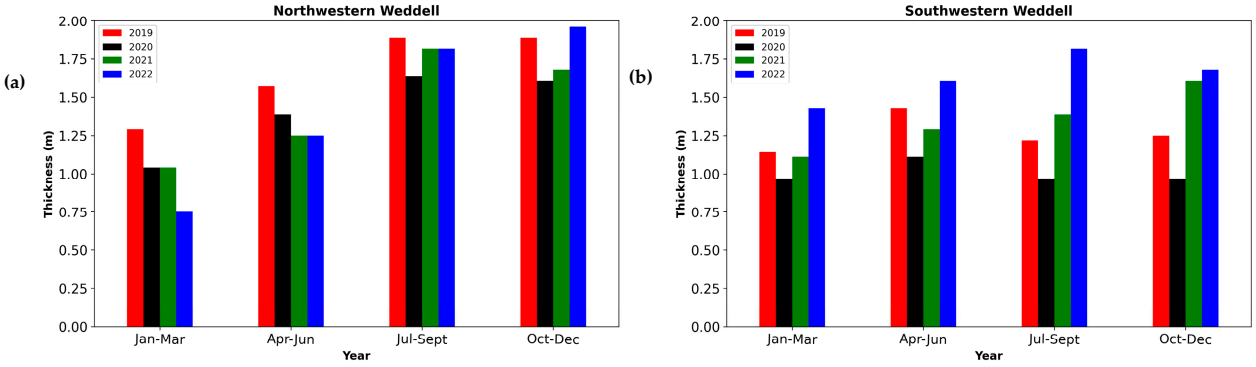

Figure 5. Mean thickness from (**a**) northwestern and (**b**) southwestern Weddell Sea.

To understand the changes in the sea ice during the year 2020, as discussed in the results and Figure 5, monthly averaged air temperature data from ERA5 reanalysis data are analyzed qualitatively from 2019 to 2022. The temperature in the western Weddell region in 2020 shows higher mean temperature during the months Jan, Feb and Mar (Figure 6a), and this can also be seen in the mean thickness value decreasing from the previous year's summer of 2019. However, the eastern Weddell Sea ice thickness does not show any apparent pattern with temperature (Figure 6b).

Along with the comparison with the field values, the ice thickness estimates are compared with previous studies in the Weddell region using the original ICESat mission, CryoSat-2, and Operation IceBridge data [7,9]. In [9], the study discusses the sea ice motion dataset from the National Snow and Ice Data Center (NSIDC) to better understand the results of sea ice thickness. They observe the clockwise pattern during the wintertime, the Weddell Gyre. Sea ice is formed in the eastern Weddell region and is advected clockwise around the southwestern Weddell, and the older sea ice is transported towards the northwestern Weddell [28]. Thus, we observe thicker ice during winter and spring in the northwestern Weddell region. This circulation also makes western Weddell one of the regions in Antarctica where multiyear sea ice is observed [26,40]. The multiyear ice is seen in Figure 2a–p, where the higher freeboards are observed in the northwestern Weddell. The OIB and ICESat estimates of freeboard and thickness show a higher value from 2003 to 2017 in late October in the western Weddell region in [26], as compared to the ICESat-2 data in the present study. The thickness value ranges from 1.25 to 2.31 m in late October

from 2003 to 2017, and the ICESat-2 thickness from 2019 to 2022 in October ranges from 1.36 ± 1.1 to 1.87 ± 1.31 m. The limited sampling from OIB may suggest uncertainty in interpreting higher thickness values in the earlier period. The Oct-Nov values from ICESat in [5] also suggest a similar trend. The sea ice thickness range was 2.2–2.3 m for both the IceBridge and ICES in the same period, whereas the Oct-Nov period in the present study in the Weddell shows a decreased thickness value in the range of 0.98–1.88 m. The study in [23] estimates sea ice thickness from 2003 to 2009 using ICESat, and the regional averages for western and eastern Weddell are 2.17 ± 0.72 m and 1.35 ± 0.54 m, respectively. This range of thickness has decreased from 2019 to 2022, where the regional averages are 1.41 m and 0.98 m for western and eastern Weddell, respectively. Thus, there is support for a decreasing trend in the sea ice thickness from 2003–2017 to 2019–2022 (Figure 7).

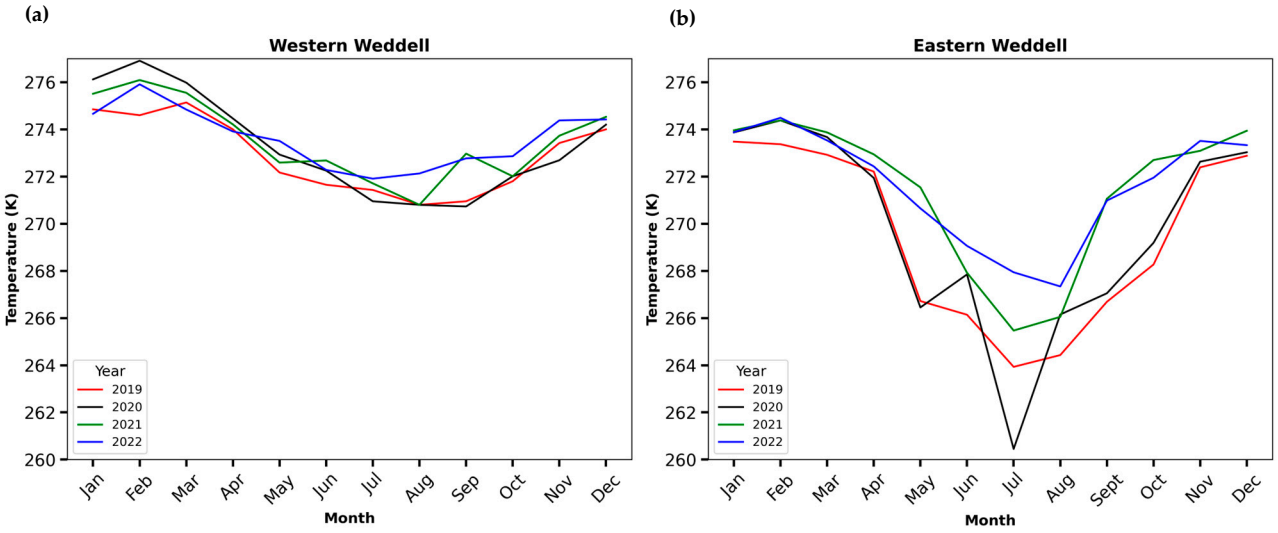

Figure 6. ERA5 monthly averaged 2 m air temperature in Kelvin for the (**a**) western and (**b**) eastern Weddell, 2019–2022.

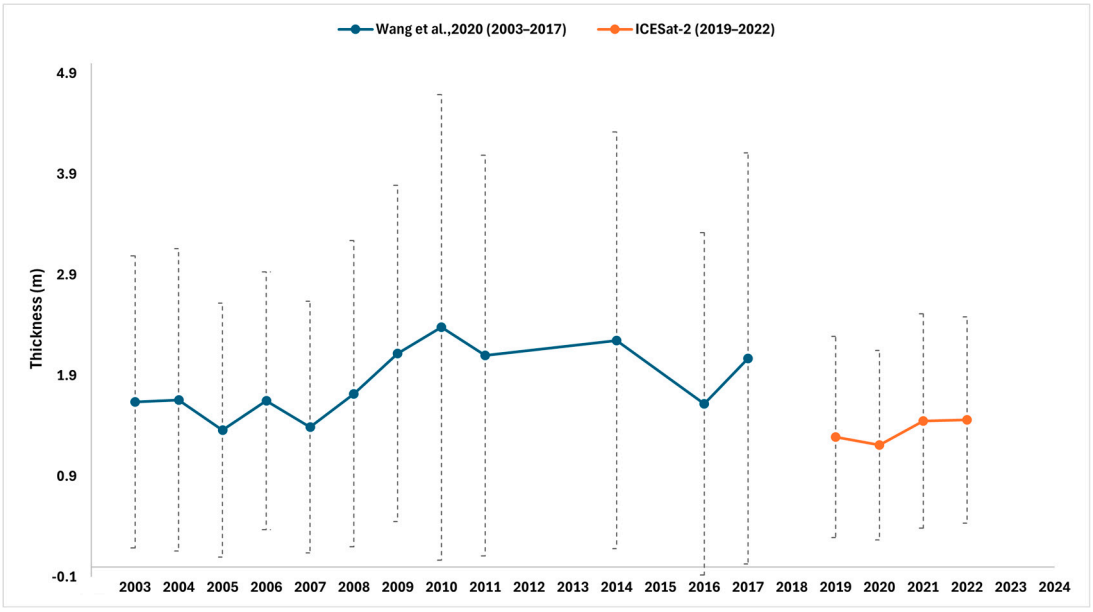

Figure 7. Comparison of ICESat and IceBridge mean thickness results in blue from [7] using the same method, with ICESat-2 results from this study in orange.

4. Conclusions

In this paper, we analyzed the sea ice thickness variations in the Weddell Sea region using ICESat-2 total freeboards from 2019 to 2022. The results were compared with the previous studies in the same region. We found that there was a decrease in the mean sea ice thickness observed from 2003–2017 to 2019–2022. Previous studies from 2003–2017 using ICESat, CryoSat-2, and OIB observed higher mean thickness values. These studies were done in the months of October and November when the sea ice reaches its maximum. However, as observed in recent years, the sea ice thickness has decreased in the same months, along with its maximum being observed in September 2023.

The interannual sea ice thickness variations observed from 2019 to 2022 demonstrate two components. First, in the summer, autumn and winter of 2020, lower mean thickness values are observed compared to the other 3 years' estimates in both western and eastern Weddell Sea. Second, there was a decrease in SIE towards the spring of 2021 and summer of 2022. These did not show a direct relation with a decrease in sea ice thickness around that time; however, the western Weddell, on further division into northwest and southwest, demonstrates a decrease in the mean thickness values in the summer of 2022. The northwest Weddell shows a decrease in thickness estimates in the summer of 2022 when compared with other years from 2019 to 2022.

In this study, we compared the field and satellite measurements with respect to snow depth, as that is one of the major uncertainties while understanding the thickness-related changes in the Antarctic region from freeboard. There is some agreement between the field and ICESat-2 data sets, but it is time- and location-dependent. Still, ICESat-2 is informative about the ice type in the region, and this information can be used to better understand the changes on a larger scale. The data used in this study are from the last four years due to the limited availability of ICESat-2, as it was launched in October 2018. As more data become available in the coming years, the evolution of ice thickness in the region could be better understood. The goal of this paper was limited to one region in Antarctica; however, this method can be applied to other regions to better understand the changes in sea ice conditions in Antarctica since 2019. This higher-resolution thickness data can be used by the modelers to better understand and predict the changes in sea ice in the future.

Author Contributions: Conceptualization, M.J., S.F.A. and A.M.M.-N.; methodology, M.J., S.F.A., A.M.M.-N. and G.J.M.; software, M.J.; validation, M.J., S.A. and C.H.; formal analysis, M.J., S.F.A., A.M.M.-N. and G.J.M.; investigation, M.J.; field resources, S.A. and C.H.; data curation, M.J.; writing—original draft preparation, M.J., S.F.A. and A.M.M.-N.; writing—review and editing, M.J., S.F.A., A.M.M.-N., G.J.M., S.A. and C.H.; visualization, M.J., S.F.A. and A.M.M.-N.; supervision, S.F.A. and A.M.M.-N.; project administration, S.F.A.; funding acquisition, M.J. and S.F.A. All authors have read and agreed to the published version of the manuscript.

Funding: M.J. was funded by NASA Future Investigator in NASA Earth and Space Science Technology (FINESST) grant number 80NSSC22K1455. S.F.A. and A.M. were supported by the Center for Advanced Measurements in Extreme Environments (CAMEE) at UTSA under NASA Grant number 80NSSC19M0194. The views and conclusions contained herein are those of the authors and should not be interpreted as necessarily the official policies or endorsements, either expressed or implied, of NASA or the U.S. Government.

Data Availability Statement: The data used in this study were obtained from the Ice, Cloud, and Land Elevation Satellite-2 (ICESat-2) mission, operated by NASA. The ICESat-2 data, including measurements of sea ice thickness, surface elevation, and other relevant parameters, are publicly available and can be accessed through the NASA National Snow and Ice Data Center (NSIDC) Distributed Active Archive Center (DAAC). The ICESat-2 ATL10 sea ice freeboard data (designated Release 005) can be obtained from the NSIDC (https://nsidc.org/data/atl10). The sea ice concentration map can be obtained from https://masie_web.apps.nsidc.org/pub/DATASETS/NOAA/G02135/south/monthly/geotiff/01_Jan/. Accessed on 7 October 2024. Snow depth data from 2019 https://doi.pangaea.de/10.1594/PANGAEA.929010. Accessed on 17 October 2024 with more details in [38], and 2021 is available on https://doi.pangaea.de/10.1594/PANGAEA.946177. Accessed on 17 October 2024. Field data from 2022 are available upon request from authors.

Acknowledgments: We acknowledge the support of the Center for Advanced Measurements in Extreme Environments (CAMEE). We would also like to acknowledge Lasse Rabenstein and his team for providing access to the Endurance 22 data during the early stages of our research. We thank the anonymous reviewers for their constructive comments.

Conflicts of Interest: The authors declare no conflicts of interest. The funders had no role in the design of the study; in the collection, analyses, or interpretation of data; in the writing of the manuscript; or in the decision to publish the results.

References

1. Ackley, S.F.; Perovich, D.K.; Maksym, T.; Weissling, B.; Xie, H. Surface flooding of Antarctic summer sea ice. *Ann. Glaciol.* **2020**, *61*, 117–126. [CrossRef]
2. Kwok, R.; Kacimi, S.; Markus, T.; Kurtz, N.T.; Studinger, M.; Sonntag, J.G.; Manizade, S.S.; Boisvert, L.N.; Harbeck, J.P. ICESat-2 Surface Height and Sea Ice Freeboard Assessed with ATM Lidar Acquisitions from Operation IceBridge. *Geophys. Res. Lett.* **2019**, *46*, 11228–11236. [CrossRef]
3. Kwok, R.; Rothrock, D.A. Decline in Arctic sea ice thickness from submarine and ICESat records: 1958–2008. *Geophys. Res. Lett.* **2009**, *36*, L15501. [CrossRef]
4. Ozsoy-Cicek, B.; Ackley, S.; Xie, H.; Yi, D.; Zwally, J. Sea ice thickness retrieval algorithms based on in situ surface elevation and thickness values for application to altimetry. *J. Geophys. Res. Oceans* **2013**, *118*, 3807–3822. [CrossRef]
5. Zwally, H.J.; Yi, D.; Kwok, R.; Zhao, Y. ICESat measurements of sea ice freeboard and estimates of sea ice thickness in the Weddell Sea. *J. Geophys. Res. Oceans* **2008**, *113*. [CrossRef]
6. Parkinson, C.L. A 40-y record reveals gradual Antarctic sea ice increases followed by decreases at rates far exceeding the rates seen in the Arctic. *Proc. Natl. Acad. Sci. USA* **2019**, *116*, 14414–14423. [CrossRef] [PubMed]
7. Wang, X.; Jiang, W.; Xie, H.; Ackley, S.; Li, H. Decadal Variations of Sea Ice Thickness in the Amundsen-Bellingshausen and Weddell Seas Retrieved from ICESat and IceBridge Laser Altimetry, 2003–2017. *J. Geophys. Res. Oceans* **2020**, *125*, e2020JC016077. [CrossRef]
8. Roach, L.A.; Meier, W.N. Sea ice in 2023. *Nat. Rev. Earth Environ.* **2024**, *5*, 235–237. [CrossRef]
9. Shi, Q.; Yang, Q.; Mu, L.; Wang, J.; Massonnet, F.; Mazloff, M.R. Evaluation of sea-ice thickness from four reanalyses in the Antarctic Weddell Sea. *Cryosphere* **2021**, *15*, 31–47. [CrossRef]
10. Morioka, Y.; Behera, S.K. Remote and Local Processes Controlling Decadal Sea Ice Variability in the Weddell Sea. *J. Geophys. Res. Oceans* **2021**, *126*, e2020JC017036. [CrossRef]
11. Maksym, T.; Jeffries, M.O. A one-dimensional percolation model of flooding and snow ice formation on Antarctic sea ice. *J. Geophys. Res. Oceans* **2000**, *105*, 26313–26331. [CrossRef]
12. Willatt, R.C.; Giles, K.A.; Laxon, S.W.; Stone-Drake, L.; Worby, A.P. Field Investigations of Ku-Band Radar Penetration Into Snow Cover on Antarctic Sea Ice. *IEEE Trans. Geosci. Remote Sens.* **2010**, *48*, 365–372. [CrossRef]
13. Fons, S.; Kurtz, N.; Bagnardi, M. A decade-plus of Antarctic sea ice thickness and volume estimates from CryoSat-2 using a physical model and waveform fitting. *Cryosphere* **2023**, *17*, 2487–2508. [CrossRef]
14. Giovinetto, M.B.; Bromwich, D.H.; Wendler, G. Atmospheric net transport of water vapor and latent heat across 70 °S. *J. Geophys. Res. Atmos.* **1992**, *97*, 917–930. [CrossRef]
15. Giles, K.A.; Laxon, S.W.; Worby, A.P. Antarctic sea ice elevation from satellite radar altimetry. *Geophys. Res. Lett.* **2008**, *35*. [CrossRef]
16. Rothrock, D.A.; Yu, Y.; Maykut, G.A. Thinning of the Arctic sea-ice cover. *Geophys. Res. Lett.* **1999**, *26*, 3469–3472. [CrossRef]
17. Li, H.; Xie, H.; Kern, S.; Wan, W.; Ozsoy, B.; Ackley, S.; Hong, Y. Spatio-temporal variability of Antarctic sea-ice thickness and volume obtained from ICESat data using an innovative algorithm. *Remote Sens. Environ.* **2018**, *219*, 44–61. [CrossRef]
18. Warren, S.G.; Rigor, I.G.; Untersteiner, N.; Radionov, V.F.; Bryazgin, N.N.; Aleksandrov, Y.I.; Colony, R. Snow depth on Arctic sea ice. *J. Clim.* **1999**, *12*, 1814–1829. [CrossRef]
19. Kern, S.; Ozsoy-Çiçek, B.; Worby, A. Antarctic Sea-Ice Thickness Retrieval from ICESat: Inter-Comparison of Different Approaches. *Remote Sens.* **2016**, *8*, 538. [CrossRef]
20. Tamura, T.; Ohshima, K.I.; Markus, T.; Cavalieri, D.J.; Nihashi, S.; Hirasawa, N. Estimation of Thin Ice Thickness and Detection of Fast Ice from SSM/I Data in the Antarctic Ocean. *J. Atmos. Oceans Technol.* **2007**, *24*, 1757–1772. [CrossRef]
21. Martin, S.; Drucker, R.S.; Kwok, R. The areas and ice production of the western and central Ross Sea polynyas, 1992–2002, and their relation to the B-15 and C-19 iceberg events of 2000 and 2002. *J. Mar. Syst.* **2007**, *68*, 201–214. [CrossRef]
22. Kaleschke, L.; Tian-Kunze, X.; Hendricks, S.; Ricker, R. SMOS-derived Antarctic thin sea ice thickness: Data description and validation in the Weddell Sea. *Earth Syst. Sci. Data* **2024**, *16*, 3149–3170. [CrossRef]
23. Wang, J.; Min, C.; Ricker, R.; Shi, Q.; Han, B.; Hendricks, S.; Wu, R.; Yang, Q. A comparison between Envisat and ICESat sea ice thickness in the Southern Ocean. *Cryosphere* **2022**, *16*, 4473–4490. [CrossRef]
24. Kurtz, N.T.; Markus, T. Satellite observations of Antarctic sea ice thickness and volume. *J. Geophys. Res. Oceans* **2012**, *117*, C08025. [CrossRef]

25. Xie, H.; Tekeli, A.E.; Ackley, S.F.; Yi, D.; Zwally, H.J. Sea ice thickness estimations from ICESat Altimetry over the Bellingshausen and Amundsen Seas, 2003–2009. *J. Geophys. Res. Oceans* **2013**, *118*, 2438–2453. [CrossRef]
26. Yi, D.; Zwally, H.J.; Robbins, J.W. ICESat observations of seasonal and interannual variations of sea-ice freeboard and estimated thickness in the Weddell Sea, Antarctica (2003–2009). *Ann. Glaciol.* **2011**, *52*, 43–51. [CrossRef]
27. Neumann, T.A.; Martino, A.J.; Markus, T.; Bae, S.; Bock, M.R.; Brenner, A.C.; Brunt, K.M.; Cavanaugh, J.; Fernandes, S.T.; Hancock, D.W.; et al. The Ice, Cloud, and Land Elevation Satellite—2 Mission: A Global Geolocated Photon Product Derived from the Advanced Topographic Laser Altimeter System. *Remote Sens. Environ.* **2019**, *233*, 111325. [CrossRef]
28. Kacimi, S.; Kwok, R. The Antarctic sea ice cover from ICESat-2 and CryoSat-2: Freeboard, snow depth, and ice thickness. *Cryosphere* **2020**, *14*, 4453–4474. [CrossRef]
29. Kwok, R.; Cunningham, G.F.; Markus, T.; Hancock, D.; Morison, J.; Palm, S.; Farrell, S.; Ivanoff, A.; Wimert, J. ATLAS/ICESat-2 User Guide. In *ATLAS/ICESat-2 L3A Sea Ice Height, Version 1*; NSIDC National Snow and Ice Data Center: Boulder, CO, USA, 2019. [CrossRef]
30. Kwok, R.; Markus, T.; Kurtz, N.T.; Petty, A.A.; Neumann, T.A.; Farrell, S.L.; Cunningham, G.F.; Hancock, D.W.; Ivanoff, A.; Wimert, J.T. Surface Height and Sea Ice Freeboard of the Arctic Ocean from ICESat-2: Characteristics and Early Results. *J. Geophys. Res. Oceans* **2019**, *124*, 6942–6959. [CrossRef]
31. Fons, S.W.; Kurtz, N.T.; Bagnardi, M.; Petty, A.A.; Tilling, R.L. Assessing CryoSat-2 Antarctic Snow Freeboard Retrievals Using Data from ICESat-2. *Earth Space Sci.* **2021**, *8*, e2021EA001728. [CrossRef]
32. Xie, H.; Ackley, S.F.; Yi, D.; Zwally, H.J.; Wagner, P.; Weissling, B.; Lewis, M.; Ye, K. Sea-ice thickness distribution of the Bellingshausen Sea from surface measurements and ICESat altimetry. *Deep Sea Res. Part II Top. Stud. Oceanogr.* **2011**, *58*, 1039–1051. [CrossRef]
33. Petty, A.A.; Kurtz, N.T.; Kwok, R.; Markus, T.; Neumann, T.A. Winter Arctic Sea Ice Thickness from ICESat-2 Freeboards. *J. Geophys. Res. Oceans* **2020**, *125*, e2019JC015764. [CrossRef]
34. Sturm, M.; Holmgren, J. An Automatic Snow Depth Probe for Field Validation Campaigns. *Water Resour. Res.* **2018**, *54*, 9695–9701. [CrossRef]
35. Haas, C.; Gerland, S.; Eicken, H.; Miller, H. Comparison of sea-ice thickness measurements under summer and winter conditions in the Arctic using a small electromagnetic induction device. *Geophysics* **1997**, *62*, 749–757. [CrossRef]
36. Kovacs, A.; Morey, R.M. Sounding sea ice thickness using a portable electromagnetic induction instrument. *Geophysics* **1991**, *56*, 1992–1998. [CrossRef]
37. Worby, A.P.; Griffin, P.W.; Lytle, V.I.; Massom, R.A. On the use of electromagnetic induction sounding to determine winter and spring sea ice thickness in the Antarctic. *Cold Reg. Sci. Technol.* **1999**, *29*, 49–58. [CrossRef]
38. Haas, C. Evaluation of ship-based electromagnetic-inductive thickness measurements of summer sea-ice in the Bellingshausen and Amundsen Seas, Antarctica. *Cold Reg. Sci. Technol.* **1998**, *27*, 1–16. [CrossRef]
39. Xu, Y.; Li, H.; Liu, B.; Xie, H.; Ozsoy-Cicek, B. Deriving Antarctic Sea-Ice Thickness from Satellite Altimetry and Estimating Consistency for NASA's ICESat/ICESat-2 Missions. *Geophys. Res. Lett.* **2021**, *48*, e2021GL093425. [CrossRef]
40. Lange, M.A.; Eicken, H. The sea ice thickness distribution in the northwestern Weddell Sea. *J. Geophys. Res. Oceans* **1991**, *96*, 4821–4837. [CrossRef]
41. Holland, P.R.; Kwok, R. Wind-driven trends in Antarctic sea-ice drift. *Nat. Geosci.* **2012**, *5*, 872–875. [CrossRef]
42. Arndt, S.; Haas, C.; Meyer, H.; Peeken, I.; Krumpen, T. Recent observations of superimposed ice and snow ice on sea ice in the northwestern Weddell Sea. *Cryosphere* **2021**, *15*, 4165–4178. [CrossRef]
43. Turner, J.; Holmes, C.; Harrison, T.C.; Phillips, T.; Jena, B.; Reeves-Francois, T.; Fogt, R.; Thomas, E.R.; Bajish, C.C. Record Low Antarctic Sea Ice Cover in February 2022. *Geophys. Res. Lett.* **2022**, *49*, e2022GL098904. [CrossRef]